

# Non-Gaussianity and the CMB Bispectrum: confusion between Primordial and Lensing-Rees Sciama contribution?

Anna Mangilli<sup>1</sup>, Licia Verde<sup>1,2</sup>

<sup>1</sup> *Institute of Space Sciences (IEEC-CSIC), Fac. Ciències, Campus UAB, Bellaterra, Spain*

<sup>2</sup> *ICREA (Institució Catalana de Recerca i Estudis Avançats)*

We revisit the predictions for the expected Cosmic Microwave Background bispectrum signal from the primordial-lensing-Rees-Sciama correlation; we point out that it can be a significant contaminant to the bispectrum signal from primordial non-Gaussianity of the local type. This non-Gaussianity, usually parameterized by the non-Gaussian parameter  $f_{NL}$ , arises for example in multi-field inflation. In particular both signals are frequency independent, and are maximized for nearly squeezed configurations. While their detailed scale-dependence and harmonic imprints are different for generic bispectrum shapes, we show that, if not included in the modeling, the primordial-lensing-Rees-Sciama contribution yields an effective  $f_{NL}$  of 10 when using a bispectrum estimator optimized for local non-Gaussianity. Considering that expected errors on  $f_{NL}$  are  $\ll 10$  from forthcoming experiments, we conclude that the contribution from this signal must be included in future constraints on  $f_{NL}$  from the Cosmic Microwave Background bispectrum.

PACS numbers:

## I. INTRODUCTION

The increased sensitivity of the forthcoming Cosmic Microwave Background (CMB) experiments will open the possibility to detect higher-order correlations in the CMB temperature fluctuations beyond the power spectrum. This means that it would be possible to study in detail eventual deviations from Gaussian initial conditions and thus gain a unique insight into the physics of the early universe (see e.g. [1] for a review). Since gravitationally induced non-linearities are small at last scattering, the CMB is expected to be the best probe of the primordial non-Gaussianity (e.g., [2, 3]).

Moreover, even in absence of these primordial deviations, measuring the three-point correlation function or, equivalently its Fourier analogue, the angular bispectrum, would be very useful to trace the imprint of the non-linear growth of structures on secondary anisotropies and would open a new window into the understanding of the evolution and growth of structures. The expected bispectrum signature of secondary CMB anisotropies has been studied in e.g., [4, 5, 6, 7, 8, 9, 10].

After galactic foregrounds, point sources and the Sunyaev-Zeldovich signature from clusters are expected to be the dominant source of non-Gaussianity in CMB data. At  $\ell < 1500$  the statistical properties of these two contributions is expected to be quite similar: both are expected to behave as an extra Poisson contribution (see [11] for treatment). In addition, both signals have a well known frequency dependence that can be used to clean CMB maps from this contaminating signal.

In [7] it was shown that the leading contribution to the CMB bispectrum with a blackbody frequency dependence is that of the primordial-lensing-Rees Sciama correlation. They also computed the expected signal-to-noise for this effect and found that experiments such a

Planck<sup>1</sup> or ACT<sup>2</sup> should be able to obtain a high statistical significance detection. This was then independently confirmed by [12, 13].

Sparked by a recent study claiming a more than 95% confidence limit detection [14], but see [15, 16, 17, 18], the subject of primordial non-Gaussianity has received renewed attention. We are thus motivated to revisit the predictions for the expected bispectrum signal from the primordial-lensing-Rees Sciama correlation in light of new developments since the year 2000: a much better-determined fiducial cosmological model with a lower  $\sigma_8$ , improved description of linear and non-linear evolution of clustering in the presence of dark energy, optimized estimators for primordial non-Gaussianity via the bispectrum signal and the tantalizing hint of a possible detection. We will also explore whether the primordial-lensing-Rees Sciama could have been confused with primordial signal and examine possible ways to separate the signals.

The rest of the paper is organized as follows: in Sec. II we review the basic of the primary CMB bispectrum and of the primordial-lensing-Rees Sciama one. In Sec. III we present numerical results for the expected signal-to-noise, the dependence of the signal on bispectrum shape and we quantify the dependence of the secondary bispectrum signal on different descriptions for non-linear evolution of clustering. In Sec. IV we explore a possible confusion between the two bispectra and prospects for separating the signals. Finally we conclude in Sec. V. Useful formulae are reported in the Appendix.

---

<sup>1</sup> [www.rssd.esa.int/Planck](http://www.rssd.esa.int/Planck)

<sup>2</sup> <http://www.physics.princeton.edu/act/>

## II. THE PRIMORDIAL AND THE SECONDARY LENSING-REES-SCIAMA CMB BISPECTRUM

In this section we review the necessary background and the basic description of the primordial CMB angular bispectrum and the secondary one arising from the cross correlation among the primordial-lensing-Rees Sciamia (LRS) contributions. For the primordial non-Gaussianity we will consider the so-called *local* type characterized by a momentum-independent non-Gaussian parameter  $-f_{NL}$  and refer to [1, 6, 11]. In reviewing the secondary LRS bispectrum we mainly follow [5, 7, 12].

### A. The Primordial CMB bispectrum

The standard single-field slow-roll inflation model predicts a non-Gaussianity of the form [2, 11, 19, 20]

$$\Phi(\mathbf{x}) = \Phi_L(\mathbf{x}) + f_{NL}(\Phi_L^2(\mathbf{x}) - \langle \Phi_L^2(\mathbf{x}) \rangle), \quad (1)$$

where  $\Phi(\mathbf{x})$  denotes the Bardeen potential,  $\Phi_L(\mathbf{x})$  denotes the linear Gaussian part of the perturbation and the  $f_{NL}$  is a merely multiplicative constant that quantify the level of non-Gaussianity.

In standard inflation  $f_{NL}$  is unmeasurably small (less than  $10^{-6}$  [21, 22]). Within this picture, the 3-point correlation function (or equivalently, the bispectrum) turns out to be the most sensitive observable to constrain possible departures from these (nearly Gaussian) initial conditions e.g., [2]. A detection of a non-vanishing primordial bispectrum would be then the smoking gun of a different scenario describing the mechanism responsible for the generation of the primordial density perturbations.

In order to study higher-order statistics and model small deviations from Gaussianity, one can define the 3-point correlation function of Bardeen's curvature perturbations<sup>3</sup> in momentum space,  $\Phi(\mathbf{k})$ , as:

$$\langle \Phi(\mathbf{k}_1)\Phi(\mathbf{k}_2)\Phi(\mathbf{k}_3) \rangle = (2\pi)^3 \delta^3(\mathbf{k}_1 + \mathbf{k}_2 + \mathbf{k}_3) F(k_1, k_2, k_3),$$

where the function  $F(k_1, k_2, k_3)$  describes the correlation among the modes and depends on the shape of the  $(\mathbf{k}_1, \mathbf{k}_2, \mathbf{k}_3)$  triangle in momentum space. Different models make different predictions for the function  $F$ , depending on the mechanism of production of such a correlation [23, 24].

There are two main, physically-motivated classes [25]:

*i)* Local form (Squeezed configurations).

This non-Gaussianity arises from the non-linear relation between the light scalar field (different from the inflaton) driving the perturbations and the observed  $\Phi$ . In the weak non-linear coupling case the non-Gaussianity can be parametrized in real space as in Eq. (1) with  $f_{NL}$

quantifying the “level” of non-linearity. Being *local* in position space, it couples Fourier modes far outside the horizon. The signal is maximal for squeezed triangle configurations with the coupling of one large-scale mode with two small scale modes. Examples of this class of models can be the curvaton scenario [26] or the Ekpyrotic model [27, 28].

*ii)* Non-local form (Equilateral configurations).

In this case the correlation among modes is due to higher derivative operators for single field models with non-minimal coupled Lagrangian. Such a correlation is strong for modes with comparable wavelength so that the signal is maximal for equilateral configurations. Examples of models of this kind are the ghost inflation [29] and the DiracBornInfeld (DBI) [30] models among others.

In the following we will focus on the the first class of models in the simplest weak non-linear coupling case and thus we will use the parametrization of Eq. (1). Note that the non-linearity parameter  $f_{NL}$  defines the non-Gaussianity in the gravitational potential and not in the CMB temperature fluctuations. In this section we then summarize the equations that describe how the perturbations in the gravitational potential translate into the second-order perturbations of the CMB temperature, giving rise to a non-vanishing primordial CMB bispectrum.

For adiabatic scalar perturbations the primordial contribution to the CMB coefficients can be written as:

$$a_{lm}^P = 4\pi(-i)^\ell \int \frac{d^3\mathbf{k}}{(2\pi)^3} \Phi(\mathbf{k}) g_{T\ell}(k) Y_{\ell m}^*(\hat{\mathbf{n}}), \quad (2)$$

where  $g_{T\ell}(k)$  is the radiation transfer function and  $\Phi(\mathbf{k})$  is the primordial curvature perturbation in Fourier space. From this equation is clear that if any non-Gaussianity in  $\Phi(\mathbf{k})$  will appear in the  $a_{lm}^P$ . According to Eq. (1), we can decompose the curvature perturbation into a linear and non-linear term:  $\Phi(\mathbf{k}) = \Phi_L(\mathbf{k}) + \Phi_{NL}(\mathbf{k})$  and, similarly, we will have:  $a_{lm} = a_{lm}^L + a_{lm}^{NL}$ .

The  $\Phi(\mathbf{k})$ -field bispectrum will thus have contributions of the form:

$$\begin{aligned} \langle \Phi_L(\mathbf{k}_1)\Phi_L(\mathbf{k}_2)\Phi_{NL}(\mathbf{k}_3) \rangle = \\ = 2f_{NL} (2\pi)^3 P_\Phi(k_1)P_\Phi(k_2)\delta^3(\mathbf{k}_1 + \mathbf{k}_2 + \mathbf{k}_3). \end{aligned} \quad (3)$$

where we have used the definition of the Bardeen's potential linear power spectrum<sup>4</sup>  $P_\Phi(k)$ :  $\langle \Phi_L(\mathbf{k}_1)\Phi_L(\mathbf{k}_2) \rangle = (2\pi)^3 P_\Phi(k_1)\delta^3(\mathbf{k}_1 + \mathbf{k}_2)$ .

Following the steps outlined in appendix A, the primordial CMB angular bispectrum takes the form [11]:

$$\begin{aligned} B_{l_1 l_2 l_3}^{m_1 m_2 m_3 (P)} = 2\mathcal{G}_{l_1 l_2 l_3}^{m_1 m_2 m_3} \int_0^\infty r^2 dr [b_{l_1}^L(r)b_{l_2}^L(r)b_{l_3}^{NL}(r) \\ + b_{l_1}^L(r)b_{l_2}^{NL}(r)b_{l_3}^L(r) + b_{l_1}^{NL}(r)b_{l_2}^L(r)b_{l_3}^L(r)], \end{aligned}$$

<sup>3</sup> Note that the Newtonian gravitational potential  $\phi$  has the opposite sign of Bardeen's curvature perturbations:  $\Phi = -\phi$

<sup>4</sup> Recall that  $\langle \Phi_L^2(\mathbf{x}) \rangle = (2\pi)^{-3} \int d^3\mathbf{k} P_\Phi(k)$

where  $\mathcal{G}_{\ell_1\ell_2\ell_3}^{m_1m_2m_3}$  defines the Gaunt integral (see eq. (A10)) and

$$b_\ell^L(r) \equiv \frac{2}{\pi} \int_0^\infty k^2 dk P_\Phi(k) g_{T\ell}(k) j_\ell(kr), \quad (4)$$

$$b_\ell^{\text{NL}}(r) \equiv \frac{2}{\pi} \int_0^\infty k^2 dk f_{\text{NL}} g_{T\ell}(k) j_\ell(kr), \quad (5)$$

with  $j_\ell(kr)$  being the spherical Bessel functions. It is important to note that this formula is valid only when  $f_{\text{NL}}$  does not depend on the scale and it approximately applies if such a dependence is weak.

Finally, it is useful to define the primordial reduced bispectrum factorizing the  $f_{\text{NL}}$  parameter:  $b_{\ell_1\ell_2\ell_3}^P = f_{\text{NL}} \hat{b}_{\ell_1\ell_2\ell_3}^P$ , where the quantity  $\hat{b}_{\ell_1\ell_2\ell_3}^P$  is the reduced bispectrum for  $f_{\text{NL}} \equiv 1$ :

$$\hat{b}_{\ell_1\ell_2\ell_3}^P = B_{\ell_1\ell_2\ell_3}^{m_1m_2m_3(P)} |_{f_{\text{NL}}=1} (\mathcal{G}_{\ell_1\ell_2\ell_3}^{m_1m_2m_3})^{-1}. \quad (6)$$

### B. Secondary bispectra: the cross correlation between Lensing and the RS effect

The path of the CMB photons traveling from the last scattering surface can be modified by the gravitational fluctuations along the line-of-sight in several different ways. On angular scales much larger than arcminute scale the photon's geodesic is deflected by to gravitational lensing and non-linear growth and late time decay of the gravitational potential induce secondary anisotropies known as the Integrated Sachs Wolfe (ISW) [31] and the Rees-Sciama (RS) effect [32].

In this work we will concentrate on the cross correlation of the CMB lensing signal with the secondary anisotropies arising from the Rees-Sciama effect (L-RS). A closely related effect was investigated in [10], where the (linear) ISW contribution is included. After galactic foregrounds, point sources and the Sunyaev-Zeldovich [33] signature from galaxy clusters are expected to be the dominant contribution to the CMB bispectrum, but because of their frequency dependence and their statistical properties they can be separated out without major loss of information [11, 34]. The next leading bispectrum contribution is the L-RS one, which cannot be separated out by frequency dependence. Both, lensing and the RS effect, are in fact related to the gravitational potential and thus are correlated, leading to a non-vanishing bispectrum signal with a blackbody spectrum.

As already pointed out in previous works [5, 7, 12] the joined study of these phenomena through the CMB bispectrum is a very powerful tool, for example, to better understand linear and non-linear growth of structures, to break degeneracies between parameters arising in a power spectrum only analysis, or to possibly constrain Dark Energy equation of state or models beyond the standard  $\Lambda$ CDM.

Following [7], the CMB anisotropy in a direction  $\hat{n}$  can then be decomposed into:

$$\Theta(\hat{n}) = \Theta^P(\hat{n}) + \Theta^L(\hat{n}) + \Theta^{\text{RS}}(\hat{n}) \quad (7)$$

where  $P$  denotes primordial,  $L$  lensing (see Eq. B1) and  $\text{RS}$  Rees-Sciama.

We can thus write the bispectrum (see appendix A) as

$$B_{\ell_1\ell_2\ell_3}^{m_1m_2m_3} \equiv \langle a_{\ell_1}^{m_1} a_{\ell_2}^{m_2} a_{\ell_3}^{m_3} \rangle = \langle a_{\ell_1}^{m_1P} a_{\ell_2}^{m_2L} a_{\ell_3}^{m_3\text{RS}} \rangle + 5 \text{ Permutations}, \quad (8)$$

Following the steps outlined in Appendix B this becomes:

$$B_{\ell_1\ell_2\ell_3}^{m_1m_2m_3(L-RS)} = \mathcal{G}_{\ell_1\ell_2\ell_3}^{m_1m_2m_3} b_{\ell_1\ell_2\ell_3}^{L-RS} \quad (9)$$

where the reduced bispectrum is given by

$$b_{\ell_1\ell_2\ell_3}^{(L-RS)} = \frac{\ell_1(\ell_1+1) - \ell_2(\ell_2+1) + \ell_3(\ell_3+1)}{2} \times C_{\ell_1}^P \mathcal{Q}(\ell_3) + 5 \text{ Perm.}, \quad (10)$$

and  $C_\ell^P$  is the primordial angular CMB power spectrum. Here the quantity that contains physical information about the late universe is [5, 7, 35]:

$$\mathcal{Q}(\ell) \equiv \langle \phi_\ell^{*m} a_\ell^{\text{RS}m} \rangle \quad (11)$$

$$\simeq 2 \int_0^{z_{\text{ls}}} \frac{r(z_{\text{ls}}) - r(z)}{r(z_{\text{ls}})r(z)^3} \left[ \frac{\partial}{\partial z} P_\phi^{\text{NL}}(k, z) \right]_{k=\frac{\ell}{r(z)}} dz$$

that expresses the statistical expectation of the correlation between the lensing and the RS effect.

In the bottom-left panel of Fig. (1) we show the behavior of the absolute value of these coefficients  $|\mathcal{Q}(\ell)|$  for  $\ell$  up to 1000 (see §III for details). The cusp indicates that  $\mathcal{Q}(\ell)$  changes sign: this is due to the onset of non-linearities, which change the sign of  $\partial P_\phi / \partial z$ . Note that in linear theory such a derivative never changes sign giving  $\mathcal{Q}(\ell) > 0$  in the  $\Lambda$ -dominated regime (Integrated Sachs Wolfe effect) [10]. Therefore it is important to stress that this feature is a fingerprint of the non-linear regime behavior. The scale at which  $\mathcal{Q}(\ell)$  changes sign depends crucially on the scale at which the non-linear growth overcomes the linear effect, making the the L-RS bispectrum sensitive to cosmological parameters governing the growth of structure like  $\Omega_m$ ,  $w$  or  $\sigma_8$ .

### III. BISPECTRUM CALCULATION AND EXPECTED SIGNAL-TO-NOISE

We assume a fiducial  $\Lambda$ CDM model in agreement with the latest observational results [17] with the parameters listed in Tab. I. The L-RS bispectrum calculation, Eq. (10, 11), requires evaluation of the non linear  $P_\phi(k, z)$ . The gravitational potential  $\phi$  is related to the matter density fluctuation  $\delta$  through the Poisson equation:

$$P_\phi(k, z) = \left( \frac{3}{2} \Omega_m \right)^2 \left( \frac{H_0}{k} \right)^4 P_\delta(k, z) (1+z)^2. \quad (12)$$

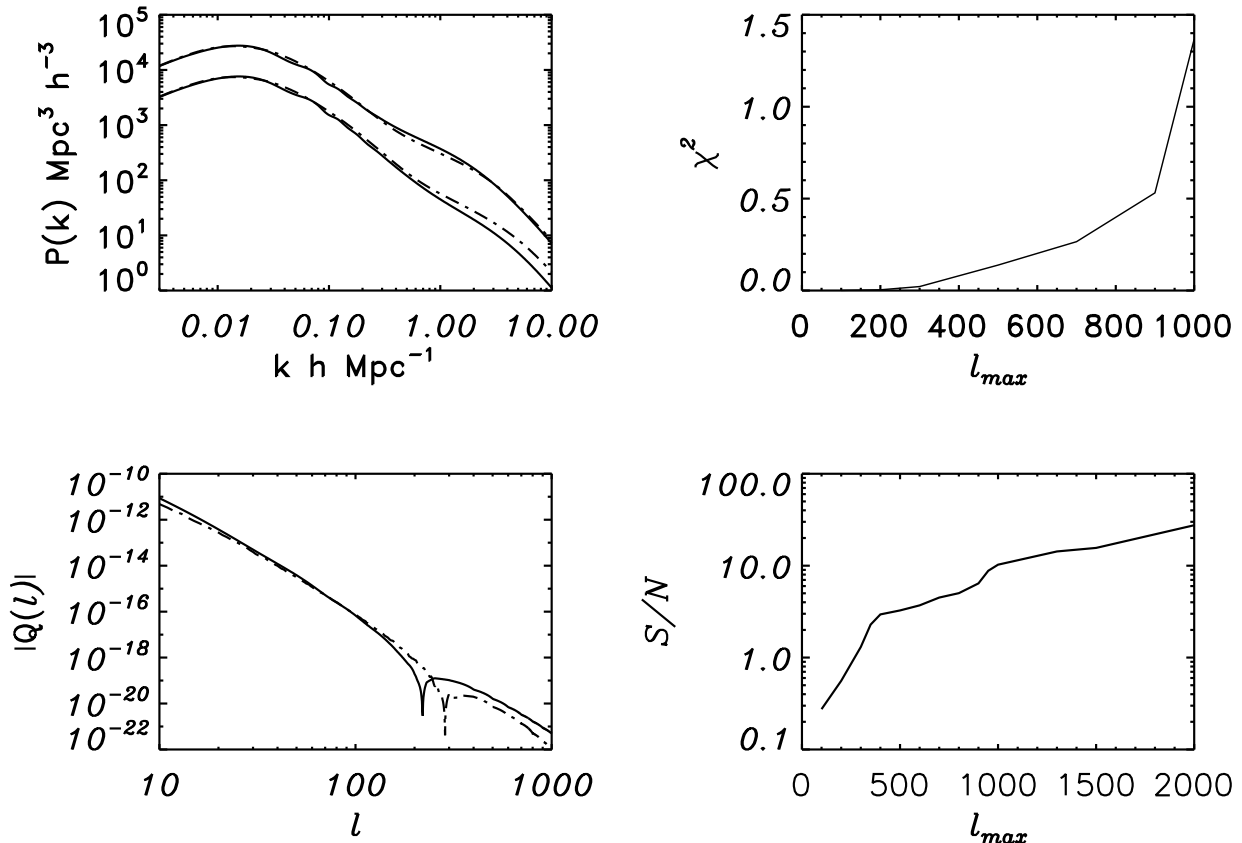


FIG. 1: TOP-LEFT panel: The non-linear matter power spectrum  $P_{\delta}^{NL}(k)$  obtained with Halofit (solid line) and by using the Peacock & Dodds (PD) semi-analytical approach (dot-dashed line). The upper curves refer to redshift  $z = 0.1$ , while the lower curves to  $z = 1$ . BOTTOM-LEFT panel: The absolute value of the  $\mathcal{Q}(\ell)$  L-RS bispectrum coefficients defined in Eq.(11), plotted as a function of the angular scale  $\ell$ . The cusp indicates where  $\mathcal{Q}$  changes sign due to the onset of non-linearities; in linear theory  $\mathcal{Q}$  is always positive. The solid line corresponds to the coefficients obtained by using the Halofit non-linear matter power spectra  $P_{\Phi}^{NL}(k, z)$ , while the dashed line refers to the  $\mathcal{Q}(\ell)$  obtained with the PD semi-analytical method to model the non-linear behavior. The cosmological parameters used are listed in tab. I. Note that the non-linear transition in the two cases happens at different scales: the  $\mathcal{Q}(\ell)$  from Halofit change sign at  $\ell \simeq 210$ , while the ones from the PD at  $\ell \simeq 300$ . BOTTOM-RIGHT panel: Signal-to-noise ratio –Eq. (13)– for the secondary Lensing-Rees Sciamia Bispectrum as a function of  $l_{max}$  in the case of an all sky, cosmic variance limited experiment. TOP-RIGHT panel:  $\chi^2$  between the L-RS bispectra obtained with Halofit and with PD as a function of the maximum multipole  $l_{max}$ .

where  $\Omega_m = \Omega_b + \Omega_c$  is the total matter density parameter. There are two approaches to compute the  $P_{\delta}^{NL}(k, z)$  that have been extensively tested and used in the literature: the more recent Halofit [36] model, which is included in CAMB [37] and the Peacock and Dodds (PD) [38] method (generalized for dark energy cosmologies by [39]). Here we use both approaches and compare them. Note that all literature so far on the L-RS bispectrum has used the PD approach to describe non-linearities.

We perform numerical derivatives to map the function  $\partial P_{\Phi}^{NL}(k, z)/\partial z$  at  $k = \frac{\ell}{r(z)}$  with  $\ell$  up to 2000. Then, to get the  $\mathcal{Q}(\ell)$  coefficients (see bottom-left panel of Fig.(1)), we numerically integrate in  $0 < z < 2.5$ , this is sufficient to account for the dark energy signature and the non-linear regime (widening the integration interval

does not change the results). For the primordial bispectrum, we proceed as in [6, 11] assuming a  $\Lambda$ CDM model. We compute the radiations transfer functions  $g_{T\ell}(k)$  with the CMBFAST code [40] and we perform the  $k$  and  $r$ -integrations in the same way [6, 11] did.

#### A. The Lensing-Rees-Sciamia bispectrum: Signal-to-Noise ratio

According to [4], the bispectrum signal-to-noise ratio can be, in general, defined as:

$$\left(\frac{S}{N}\right)^2 = \sum_{\ell_1 \ell_2 \ell_3} \frac{\langle B_{\ell_1 \ell_2 \ell_3} \rangle^2}{\Delta_{\ell_1 \ell_2 \ell_3} C_{\ell_1} C_{\ell_2} C_{\ell_3}}, \quad (13)$$

TABLE I:  $\Lambda$ CDM parameters.

Symbol	Description	Value
$H_0$	Hubble constant	70 Km/sec/Mpc
$\Omega_b$	Baryon density	0.044
$\Omega_c$	Dark matter density	0.224
$\Omega_\Lambda$	Dark energy density	0.732
$w$	Dark energy equation of state	-1
$\sigma_8$	Fluctuation amplitude at $8h^{-1}$ Mpc	0.834
$n_s$	Scalar spectral index	1
$z_{ls}$	Redshift of decoupling	1090.51

where  $\Delta_{\ell_1\ell_2\ell_3}$  is a number which takes value 6 for equilateral configurations, 2 for isosceles configurations and 1 otherwise. Following [41], the explicit expression for the variance, in the hypothesis of small departure from Gaussianity, is given in equation (A14).

Using Eq. (A12) we can write the the signal at numerator as:

$$\langle B_{\ell_1\ell_2\ell_3} \rangle^2 = \frac{(2\ell_1 + 1)(2\ell_2 + 1)(2\ell_3 + 1)}{4\pi} \times \begin{pmatrix} \ell_1 & \ell_2 & \ell_3 \\ 0 & 0 & 0 \end{pmatrix}^2 b_{\ell_1\ell_2\ell_3}^2. \quad (14)$$

The bottom-right panel of Fig. 1 shows the signal-to-noise ratio for the L-RS bispectrum as a function of the maximum multipole  $\ell_{max}$  ( $\ell_1$ ,  $\ell_2$  and  $\ell_3$  are all  $< \ell_{max}$ ). We do not consider  $\ell_{max} > 2000$  because of other secondary effects (e.g., Ostriker-Vishniac or Kinetic SZ [33, 42, 43]). The S/N plotted has been then obtained by summing over all triangle configurations for a full sky, ideal, cosmic variance-dominated experiment. The results can be representative of an experiment with the nominal performance of Planck, as pointed out in previous works [13, 44].

The signal-to-noise ratio increases mainly when the maximum multipole  $\ell_{max}$  reaches few hundred, where the L-RS signal gives the main contribution. As we will explore in more detail later on, the L-RS bispectrum signal dominates for squeezed triangle configurations when a large scale mode couples with two small scales modes: 50% of the signal-to-noise comes from triangles with  $2 \leq \ell_{min} \leq 10$ , in agreement with the findings of [7].

## B. Modeling non-linearities: Peacock & Dodds and the Halofit model

The two main approaches that can be used to compute the non-linear matter power spectrum  $P_\delta^{NL}(k)$  are the commonly used semi-analytical Peacock & Dodds [38] (PD) formula, based on the scaling method of [45], and the more recent Halofit model [36].

The first approach is based on the ansatz that the non-linear evolution induce a change of scale so that the non-linear power spectrum at wavenumber  $k$  can be parameterized by a simple function of the linear one evaluated at  $k'$ . This has been shown to interpolate correctly the  $P(k)$  behavior in the intermediate regime between linear and stable clustering.

The second approach is based on the so-called "halo model" for the matter power spectrum. In the halo model the density field is decomposed into a distribution of clumps of matter with some density profile. The large scale behavior is then derived through the correlations between different haloes, while the non-linear correlation functions on small scales are obtained from the convolution of the density profile of the halo with itself. Halofit has been also extensively tested on large, high-resolution N-body simulations.

We estimate that any uncertainty in the description of the non-linear clustering should be at or below the level of the difference between these two approaches.

In the top-left panel of Fig. 1 the non-linear matter power spectrum  $P_\delta^{NL}(k)$  is plotted as a function of the wavenumber  $k$  for Halofit (solid line) and for PD (dot-dashed line). The upper curves refer to power spectra at redshift  $z = 0.1$ , while the lower curves are the non-linear matter power spectra at  $z = 1$ . The Halofit power spectrum shows the Baryon Acoustic Oscillation (BAO) at the typical BAO scale  $k \simeq 0.1$ Mpc. To produce the PD one we started from a "no-wiggle" linear power spectrum. This is because the PD approach maps linear scales into non-linear ones thus artificially changes the position of the wiggles; when taking derivatives this can induce spurious signal which does not happen when starting from a "no-wiggle" linear  $P(k)$ . Beside the BAO feature, which is irrelevant for our purpose, the two models are in good agreement although at higher  $z$  the PD power spectrum seems to produce a power spectrum more non-linear than Halofit.

The bottom-left panel of Fig. 1 show the effect of this difference in the L-RS Bispectrum coefficients  $\mathcal{Q}(\ell)$ . The figure shows the absolute value of the coefficients  $|\mathcal{Q}(\ell)|$  as a function of the angular scale  $\ell$ . The solid line corresponds to the coefficients obtained by using Halofit while the dashed line using PD. The transition to the non-linear regime (indicated by the cusp where  $\mathcal{Q}(\ell)$  changes sign) happens at smaller  $\ell$  for Halofit ( $\simeq 200$ ) than for PD case ( $\ell \simeq 300$ ).

We quantify the difference between the two models by computing the  $\chi^2$  for the L-RS bispectra obtained respectively with Halofit and with PD:

$$\chi_{Halofit-P\&D}^2 = \sum_{\ell_1\ell_2\ell_3} \frac{B_{\ell_1\ell_2\ell_3}^{L-RS[Halofit]} - B_{\ell_1\ell_2\ell_3}^{L-RS[P\&D]}}{\Delta_{\ell_1\ell_2\ell_3} C_{\ell_1} C_{\ell_2} C_{\ell_3}} \quad (15)$$

This is shown in the top-right panel of Fig. 1 as a function of the maximum multipole  $\ell_{max}$  for our fiducial cosmology. The two models are compatible within  $1-\sigma$  ( $\Delta\chi^2 < 1$ ) for  $\ell_{max} < 900$ . We conclude that the

significance of a detection of this signal does not depend crucially on the modeling for non-linearities, however the choice of an incorrect modeling may introduce significant biases when doing precise analysis, as [7, 12], on key parameters, e.g.,  $w$ ,  $\sigma_8$ ,  $\Omega_m$  which are particularly sensitive to the onset of non-linearity.

For each of the parameters  $w$ ,  $\sigma_8$ ,  $\Omega_m$  we compute the bias introduced by using Halofit in the bispectrum calculation in the hypothetical case that PD was a true description of non-linearities. Around our fiducial model, the biases are at the level comparable to the  $1 - \sigma$  errors (0.3 to 0.6  $\sigma$ ). We estimate that, in any practical application, biases introduced by uncertainties in the description of non-linear clustering will be at this level or below. Ultimately,  $\partial P^{NL}/\partial z$  can be accurately evaluated with the use of N-body simulations as presented in [46], thus removing this source of bias.

#### IV. THE SHAPE-DEPENDENCE OF THE BISPECTRUM SIGNALS: PRIMORDIAL VS L-RS

The signal for the primordial bispectrum is dominated by squeezed and nearly squeezed configurations as shown by [25, 47]. We find that the same applies to the L-RS bispectrum, where 90% of the signal-to-noise comes from nearly squeezed configurations where  $\ell_2 > 10\ell_1$  and  $\ell_2 < \ell_3$ . This can lead to “confusion” between the two signals. We illustrate this point by defining an “effective”  $f_{NL}$  for the L-RS signal as

$$f_{NL}^{L-RS} = \frac{b_{\ell_1\ell_2\ell_3}^{L-RS}}{\hat{b}_{\ell_1\ell_2\ell_3}^P}, \quad (16)$$

which depends on triangle shape. This is shown in the left panels of Fig. 2 while the right panels show the corresponding reduced bispectra (solid for L-RS and dashed for Primordial). The top panels are for nearly-squeezed configurations where  $\ell_1$  is fixed,  $\ell_1 = 2$ ,  $\ell_2$  varies by only for  $\ell_2 > 40$ , and  $\ell_3 = \ell_2 + 2$  while the bottom panels are for isosceles squeezed configurations:  $\ell_1 = 2$ ,  $\ell_2 > 40$ ,  $\ell_3 = \ell_2$ . Note that in the right panels the primordial bispectrum has been computed for  $f_{NL} = -10$  for making it more visible.

The case of the squeezed isosceles configurations (where  $\ell_2 \gg \ell_1$ ,  $\ell_3 = \ell_2$  and  $\ell_1 < \sim 150$ ), contributes with a  $\simeq 5\%$  to the total  $S/N$  in both cases, and the two bispectra have exactly the same shape and they completely degenerate for a  $f_{NL} \simeq -17$ . For nearly squeezed-configurations  $f_{NL}^{L-RS}$  oscillates but its average is at around  $f_{NL}^{L-RS} \sim 10$ . Nearly squeezed configurations where  $\ell_2 > 10\ell_1$  and  $\ell_2 < \ell_3$  carry most of the  $S/N$ . The L-RS signal always dominates over the primordial one for all the high signal-to-noise configurations by a factor of 10-20 in absolute value.

However, besides to the fact that the two bispectra could be confused for showing some similar behavior (see

bottom panels of Fig. 2 they can in principle be disentangled since they have intrinsically different features arising from the extremely different physics behind them.

For example, looking back at the top-right panel of Fig. 2, we find that for these configurations the L-RS signal oscillate, while the Primordial reduced bispectrum does not. The L-RS bispectrum of eq. (10) in fact contains the  $C_\ell$ , with the typical structure given by the acoustic peaks, and the coefficient  $Q_\ell$  which determine the change of sign. On the other hand, the primordial signal, see eq. (4), is composed by the coefficients:  $b_\ell^L(r) \propto P_\phi(k)g_{T\ell}(k)$  and  $b_\ell^{NL}(r) \propto f_{NL}g_{T\ell}(k)$  so that the changing of sign in this case is due to the full radiation transfer functions  $g_{T\ell}(k)$ . For general configurations, the two bispectra behave differently: in Fig. 3 we plot the case of equilateral (left panel) and flattened configurations of the type:  $\ell_1 = 2\ell_3$  and  $\ell_2 = \ell_3$  (right panel). The dashed lines refers to the Primordial contribution while the solid lines to the L-RS one. The two bispectra have different shapes and change sign at different angular scales. In the case of equilateral configurations, for example, the Primordial reduced bispectrum shows the known oscillatory shape, as found in [11], while the L-RS reduced bispectrum does not. In the case of flattened configurations both bispectra show oscillations. Note that in these plots the y-axis has been multiplied by a factor  $10^{16}$  (while in Fig. (2) the y-axis has been multiplied by a factor  $10^{11}$ ): these contributions are clearly subdominant by about 5 orders of magnitude with respect to the squeezed configurations, which explains why the latter shapes dominate the signal-to-noise.

In light of these findings we now attempt to interpret recent constraints on primordial non-Gaussianity from CMB data e.g., [14, 16, 17] and consider the implications for forthcoming measurements.

The  $f_{NL}$  estimator used in these works reduces to the one defined in [48] in the simplest case of temperature-only anisotropies, cosmic variance dominated, all sky analysis. This estimator weights the bispectrum of every triplet  $\ell_1, \ell_2, \ell_3$  by the signal to noise of the primordial bispectrum. We can thus estimate the effective  $f_{NL}$  that such an estimator would measure due to the presence of the L-RS signal defining:

$$\hat{f}_{NL} = \frac{\hat{S}}{N}, \quad (17)$$

where

$$\hat{S} = \sum_{2 \leq \ell_1 \ell_2 \ell_3} \frac{B_{\ell_1\ell_2\ell_3}^{L-RS} B_{\ell_1\ell_2\ell_3}^P}{C_{\ell_1} C_{\ell_2} C_{\ell_3}} \quad (18)$$

and

$$N = \sum_{2 \leq \ell_1 \ell_2 \ell_3} \frac{(B_{\ell_1\ell_2\ell_3}^P)^2}{C_{\ell_1} C_{\ell_2} C_{\ell_3}}. \quad (19)$$

For our fiducial cosmology, summing over all configurations we find  $f_{NL} = 10$ . Restricting the

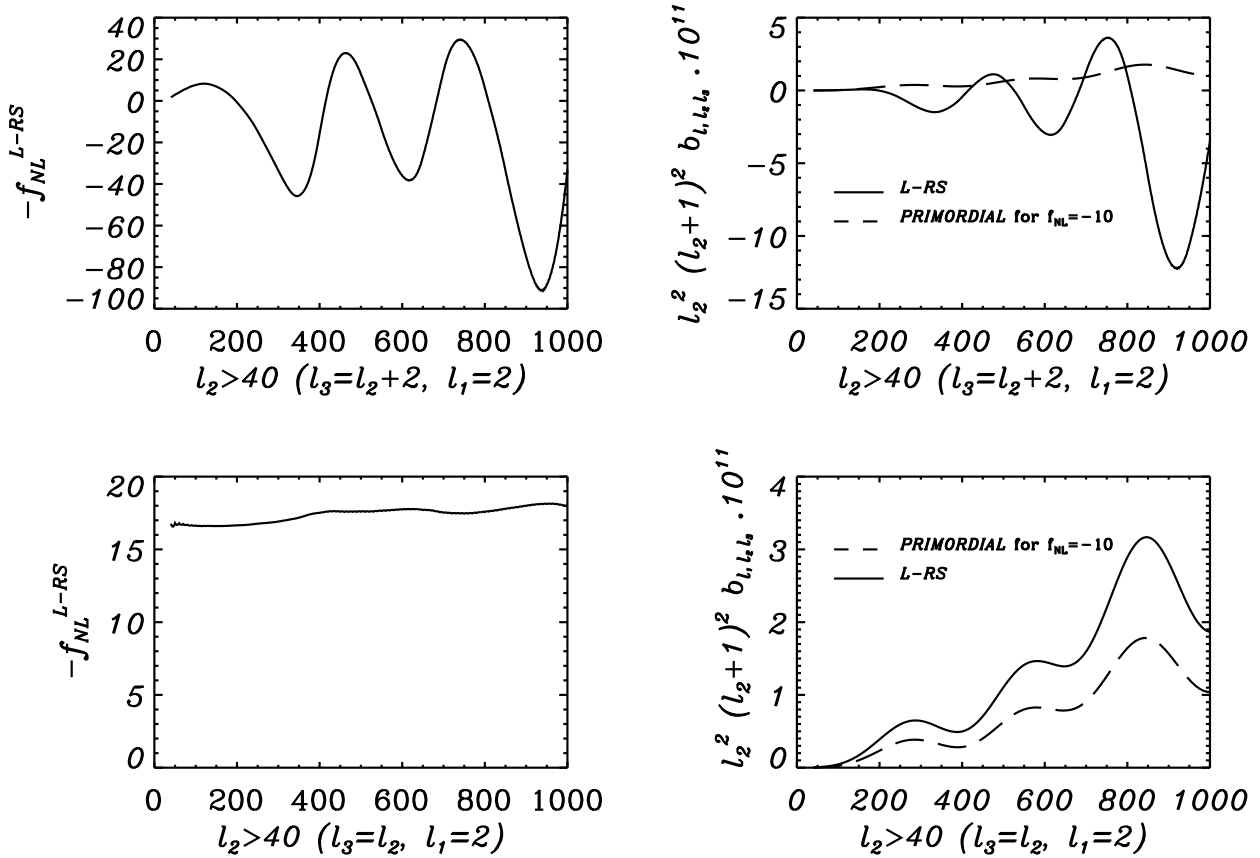


FIG. 2: Effective non-linear parameter  $f_{NL}^{L-RS}$  (Eq. 16, left panels) and corresponding reduced L-RS (solid) and Primordial (Dashed) bispectra (right panels) for two nearly squeezed configurations:  $l_1 = 2, l_2 > 40, l_3 = l_2 + 2$  (top panels) and  $l_1 = 2, l_2 > 40, l_3 = l_2$  (bottom panels). In the right panels the primordial bispectrum plotted has  $f_{NL} = -10$  for making it more visible. Note that in the case illustrated in the bottom panels, the two bispectra have exactly the same shape and they are completely degenerate for a  $f_{NL} \simeq -17$ .

sums to nearly squeezed configurations such that:  $\sum_{l_1=2}^{10} \sum_{l_2=90l_1}^{\ell_{max}=1000} \sum_{l_3=l_2}^{1000}$ , which contribute with about a 73% to the total signal-to-noise in both cases, we find  $f_{NL} = 15$ . Using Halofit or PD in the modeling of the L-RS bispectrum changes the estimates of the effective  $f_{NL}$  by 10% indicating that this correction is robust to possible residual uncertainty in the modeling of nonlinearities.

It is also possible to estimate the effective  $f_{NL}$  via a simple  $\chi^2$  analysis: we find the same values as above but the interpretation of the  $\chi^2$  as a goodness of fit test would indicate that the local model is not a good fit. This is in qualitative agreement with the findings of [49] who compute the CMB bispectrum from the second-order fluctuations and find that their effect is separable from the primordial non-Gaussian signal because of the different shape dependence for non-squeezed (or nearly squeezed) configurations. The agreement cannot be made fully quantitative as perturbation theory approach may break down: for a given multipole  $\ell$  the derivative of the grav-

itational potential power spectrum is probed at a wide range of scales  $k(z) = \frac{\ell}{r(z)}$  and therefore highly nonlinear scales can contribute non-negligibly even at relatively low  $\ell$ .

In practice, however, it may not be possible to implement a goodness of fit test, especially if the errors on  $f_{NL}$  are computed by Monte-Carlo.

The expected error on  $f_{NL}$  for forthcoming surveys is smaller than 10 (for example the Planck surveyor, recently launched is expected to yield 1- $\sigma$  error on  $f_{NL}$  of order 4 [44]), indicating that the L-RS signal may be a crucial contaminant in the pursuit of primordial non-Gaussianity, if not properly taken into account. We have shown here that its amplitude and configuration dependence is well known; it is thus not necessary to extract this signal from the CMB bispectrum and separate it from the primordial: it can simply be included in the modeling of the CMB bispectrum.

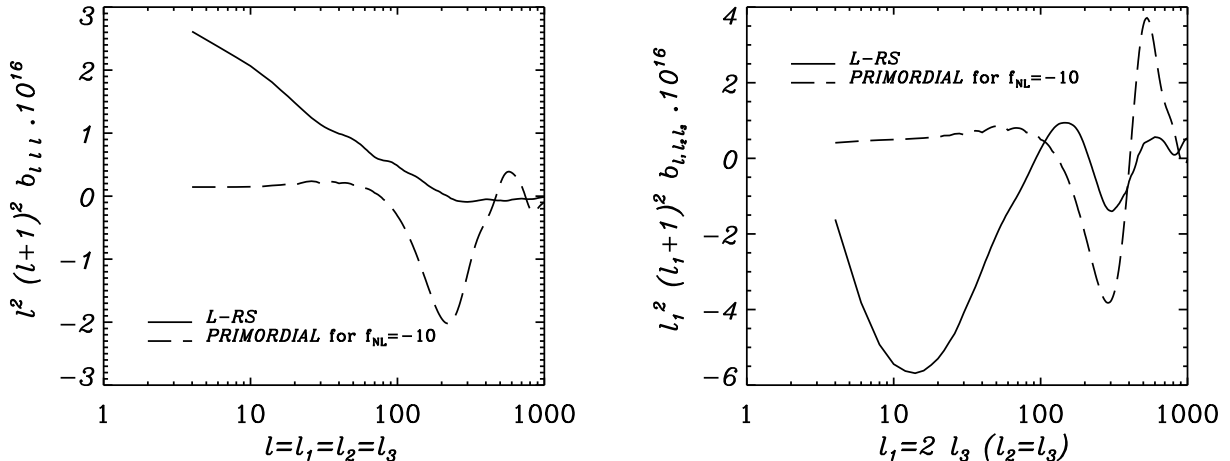


FIG. 3: Reduced bispectra  $b_{l_1 l_2 l_3}$ : Primordial for  $f_{nl} = -1$  (dashed line) and Lensing-Rees Sciamia (solid line). The left plot shows equilateral triangle configurations  $\ell = \ell_1 = \ell_2 = \ell_3$ , while the right one shows the flattened configurations  $\ell_1 = 2\ell_3$  and  $\ell_2 = \ell_3$ . We have plotted  $b_{l_1 l_2 l_3}^{L-RS} \ell_1^2 (\ell_1 + 1)^2 10^{16}$ , which makes the Sachs-Wolfe plateau of the Primordial reduced bispectrum easily seen at large angular scales.

## V. CONCLUSIONS

We have revisited the predictions for the expected CMB bispectrum signature of the primordial-lensing Rees-Sciama (L-RS) correlation. This bispectrum is the leading contribution on scales much larger than arcminute with the same frequency dependence as the CMB primary. Forthcoming experiments like Planck have the statistical power to detect this signal with a signal-to-noise of order 10. The signal depends on the balance of two competing contributions along the line of sight: the decaying gravitational potential fluctuations and the amplification due to non-linear gravity. For this reason the effect can be used to place strong constraints on cosmological parameters that determine the growth of structures:  $\Omega_m$ , dark energy parameters and  $\sigma_8$ . By comparing two different semi-analytic descriptions of non-linear clustering, we find that an accurate description of the non-linear growth of the matter power spectrum is necessary to obtain unbiased estimates of these parameters. Approaches based on numerical simulations (see e.g., [46]) will have to be employed.

We also find that this bispectrum signal can be confused with the signal from local primordial non-Gaussianity. Both bispectra signal are maximal for squeezed or nearly squeezed configurations. For some configurations (e.g., squeezed isosceles) the two bispectra are virtually identical, while for generic configurations the shape dependence of the two bispectra are different in the details. A bispectrum estimator optimized for constraining primordial non-Gaussianity of the local type would measure an effective  $f_{NL} = 10$  due to the presence of the primordial-lensing-Rees-Sciama correlation. If not accounted for, this introduces a bias in the constraints

on primordial non-Gaussianity from the CMB bispectrum. This is in qualitative agreement with the effect explored in [10] where only linear growth was included. For  $\ell > 200$  the full non-linear treatment is needed. For current data, this bias is smaller than the  $1-\sigma$  error, however it can become significant when interpreting the statistical significance of results that are at the boundary of the  $3-\sigma$  confidence level. For example if we subtract the effective value for the L-RS  $f_{NL}$  from the central value of the estimate of [14], we obtain that  $f_{NL}$  primordial is consistent to zero at the  $\sim 2.5\sigma$  confidence level. For forthcoming data, however, this bias will be larger than the  $1-\sigma$  error and thus non-negligible.

Techniques to separate out different bispectra shapes and assess whether a detection of non-Gaussianity is primordial have been proposed [50] and will be suitable for this application.

We argue that the bispectrum of the L-RS effect can be accurately modeled: even with currently available semi-analytic descriptions for non-linear clustering, we estimate the error on the effective  $f_{NL}$  to be at the 10% level or below. We conclude that, in analyzing the CMB bispectrum to obtain constraints on primordial non-Gaussianity for forthcoming data, this contribution must be included in the modeling.

While this paper was being completed a related work was posted in the on-line archive: Boubekour et al. <http://arxiv.org/pdf/0906.0980> where the secondary contributions to the CMB bispectrum due to lensing and the ISW separately has been calculated by using perturbation theory up to second order. Their results are in qualitative agreement with ours (see also [49]), the agreement however cannot be made fully quantitative because they assumed an exact matter dominance, described non-



linearities only up to second-order and did not consider the contribution coming from the cross correlation between primordial lensing and the RS effect.

### Acknowledgments

We thank Michele Liguori for invaluable help with the CMBFAST radiation transfer function. AM is supported by CSIC I3 #200750I034 and FP7-PEOPLE-2002IRG4-4-IRG#202182. LV acknowledges support of FP7-PEOPLE-2002IRG4-4-IRG#202182.

### APPENDIX A: BISPECTRUM STATISTICS

Deviations from Gaussianity in the CMB are characterized by the angular n-points correlation function of the temperature field in the sky [3]:

$$\langle \Theta(\hat{\mathbf{n}}_1)\Theta(\hat{\mathbf{n}}_2)\dots\Theta(\hat{\mathbf{n}}_n) \rangle \quad (\text{A1})$$

where the bracket defines the ensemble average and  $\hat{\mathbf{n}}$  the angular position (i.e. the direction unit vector of the incoming photons). In general it is useful to expand the field in terms of spherical harmonics:

$$\Theta(\hat{\mathbf{n}}) = \sum_{\ell=0}^{\infty} \sum_{m=-\ell}^{\ell} a_{\ell m} Y_{\ell m}(\hat{\mathbf{n}}), \quad (\text{A2})$$

so that, by using the symmetric proprieties of harmonic transformations and the orthogonality of the spherical harmonics, we can write the coefficients  $a_{\ell}^m$  as:

$$a_{\ell}^m = \int d^2\hat{\mathbf{n}} \Theta(\hat{\mathbf{n}}) Y_{\ell}^{*m}(\hat{\mathbf{n}}). \quad (\text{A3})$$

The angular CMB bispectrum is defined by three harmonic transforms satisfying rotational invariance:

$$B_{\ell_1\ell_2\ell_3}^{m_1m_2m_3} \equiv \langle a_{\ell_1m_1} a_{\ell_2m_2} a_{\ell_3m_3} \rangle, \quad (\text{A4})$$

thus the angular averaged bispectrum takes the form:

$$B_{\ell_1\ell_2\ell_3} = \sum_{\text{all } m} \begin{pmatrix} \ell_1 & \ell_2 & \ell_3 \\ m_1 & m_2 & m_3 \end{pmatrix} B_{\ell_1\ell_2\ell_3}^{m_1m_2m_3}. \quad (\text{A5})$$

Since  $\ell_1, \ell_2$  and  $\ell_3$  form a triangle, this quantity must satisfy the triangle conditions and parity invariance:

$$m_1 + m_2 + m_3 = 0, \quad \ell_1 + \ell_2 + \ell_3 = \text{even},$$

$$|\ell_i - \ell_j| \leq \ell_k \leq \ell_i + \ell_j \quad (\text{A6})$$

for all permutations of indices. The matrix appearing in equation (A5) represents the Wigner-3j symbol that describes the coupling of two angular momenta. Rotational

invariance requires the bispectrum amplitude to be independent from orientation and triangle configuration. The Wigner-3j symbol, transforming the m's under rotations, preserve the triangle configuration thus describing the bispectrum azimuthal angle dependence. The orthogonality properties of the Wigner-3j symbols are

$$\sum_{\text{all } m} \begin{pmatrix} \ell_1 & \ell_2 & \ell_3 \\ m_1 & m_2 & m_3 \end{pmatrix}^2 = 1 \quad (\text{A7})$$

$$\sum_{m'_1 m'_2} \begin{pmatrix} \ell_1 & \ell_2 & \ell_3 \\ m'_1 & m'_2 & m'_3 \end{pmatrix} \begin{pmatrix} \ell_1 & \ell_2 & L \\ m'_1 & m'_2 & M' \end{pmatrix} = \frac{\delta_{\ell_3 L} \delta_{m'_3 M'}}{2L+1} \quad (\text{A8})$$

By making use again of rotational invariance and of the symmetry and orthogonality properties of the 3-j symbols, we can write the bispectrum as:

$$B_{\ell_1\ell_2\ell_3}^{m_1m_2m_3} = \mathcal{G}_{\ell_1\ell_2\ell_3}^{m_1m_2m_3} b_{\ell_1\ell_2\ell_3} \quad (\text{A9})$$

where  $\mathcal{G}_{\ell_1\ell_2\ell_3}^{m_1m_2m_3}$  is the Gaunt integral which contains all the angle dependence and triangle constraint information and it is defined by:

$$\begin{aligned} \mathcal{G}_{\ell_1\ell_2\ell_3}^{m_1m_2m_3} &\equiv \int d^2\hat{\mathbf{n}} Y_{\ell_1 m_1}(\hat{\mathbf{n}}) Y_{\ell_2 m_2}(\hat{\mathbf{n}}) Y_{\ell_3 m_3}(\hat{\mathbf{n}}) \\ &= \sqrt{\frac{(2\ell_1+1)(2\ell_2+1)(2\ell_3+1)}{4\pi}} \\ &\times \begin{pmatrix} \ell_1 & \ell_2 & \ell_3 \\ 0 & 0 & 0 \end{pmatrix} \begin{pmatrix} \ell_1 & \ell_2 & \ell_3 \\ m_1 & m_2 & m_3 \end{pmatrix}, \end{aligned} \quad (\text{A10})$$

where  $b_{\ell_1\ell_2\ell_3}$  is called the reduced bispectrum, which is a very useful quantity since it is an arbitrary symmetric function of  $\ell_1, \ell_2$  and  $\ell_3$  only and it contains all the relevant physical information of the bispectrum.

By substituting equation(A9) into equation(A5) and using the Gaunt integral property:

$$\begin{aligned} \sum_{\text{all } m} \begin{pmatrix} \ell_1 & \ell_2 & \ell_3 \\ m_1 & m_2 & m_3 \end{pmatrix} \mathcal{G}_{\ell_1\ell_2\ell_3}^{m_1m_2m_3} &= \quad (\text{A11}) \\ &= \sqrt{\frac{(2\ell_1+1)(2\ell_2+1)(2\ell_3+1)}{4\pi}} \begin{pmatrix} \ell_1 & \ell_2 & \ell_3 \\ 0 & 0 & 0 \end{pmatrix}, \end{aligned}$$

we can finally write:

$$\begin{aligned} B_{\ell_1\ell_2\ell_3} &= \sqrt{\frac{(2\ell_1+1)(2\ell_2+1)(2\ell_3+1)}{4\pi}} \\ &\times \begin{pmatrix} \ell_1 & \ell_2 & \ell_3 \\ 0 & 0 & 0 \end{pmatrix} b_{\ell_1\ell_2\ell_3}. \end{aligned} \quad (\text{A12})$$

For high- $\ell$  the Gosper factorials approximation for the Wigner 3j symbols can be used:

$$\begin{aligned} \begin{pmatrix} \ell_1 & \ell_2 & \ell_3 \\ 0 & 0 & 0 \end{pmatrix} &\simeq \left(-\frac{L}{L+1}\right)^{L/2} \frac{1}{(6L+7)^{1/4}} \\ \left(\frac{3e}{\pi} \frac{3L+1}{L+1}\right)^{1/2} &\prod_{i=1}^3 \frac{(6L-12\ell_i+1)^{1/4}}{(3L-6\ell_i+1)^{1/2}}. \end{aligned} \quad (\text{A13})$$

Finally, we provide the explicit expression of the bispectrum variance in the hypothesis of small departure of Gaussianity:

$$\begin{aligned}
\sigma_{\ell_1 \ell_2 \ell_3}^2 &\simeq \langle B_{\ell_1 \ell_2 \ell_3}^2 \rangle = \langle a_{\ell_1}^{m_1} a_{\ell_2}^{m_2} a_{\ell_3}^{m_3} a_{\ell_1}^{m_1*} a_{\ell_2}^{m_2*} a_{\ell_3}^{m_3*} \rangle = \\
&= \mathcal{C}_{\ell_1} \mathcal{C}_{\ell_2} \mathcal{C}_{\ell_3} \\
&+ 2\mathcal{C}_{\ell_1}^3 \delta_{\ell_1 \ell_2 \ell_3} (\delta_{m_1 m_3} + \delta_{m_1 - m_3}) (\delta_{m_1 m_2} + \delta_{m_1 - m_2}) \\
&+ \mathcal{C}_{\ell_1} \mathcal{C}_{\ell_2}^2 \delta_{\ell_2 \ell_3} (\delta_{m_2 m_3} + \delta_{m_2 - m_3}) \\
&+ \mathcal{C}_{\ell_2} \mathcal{C}_{\ell_3}^2 \delta_{\ell_3 \ell_1} (\delta_{m_1 m_3} + \delta_{m_1 - m_3}) \\
&+ \mathcal{C}_{\ell_3} \mathcal{C}_{\ell_1}^2 \delta_{\ell_1 \ell_2} (\delta_{m_1 m_2} + \delta_{m_1 - m_2}).
\end{aligned} \tag{A14}$$

## APPENDIX B: WEAK LENSING OF THE CMB

Weak lensing of the CMB re-maps the temperature primary anisotropy according to:

$$\begin{aligned}
\Theta^L(\hat{\mathbf{n}}) &= \Theta^P(\hat{\mathbf{n}} + \nabla\phi) \\
&\simeq \Theta^P(\hat{\mathbf{n}}) + \nabla_i \phi(\hat{\mathbf{n}}) \nabla^i \Theta^P(\hat{\mathbf{n}}) + \dots
\end{aligned} \tag{B1}$$

where the label 'L' refers to the lensed term while 'P' to the primary contribution. The deflection angle  $\alpha = \nabla\phi$  is given by the angular gradient of the gravitational potential projection along the line of sight:

$$\phi(\hat{\mathbf{n}}) = -2 \int_0^{r_{ls}} dr \frac{r(z_{ls}) - r(z)}{r(z) r(z_{ls})} \Phi(r, \hat{n}r). \tag{B2}$$

Here  $r$  is the comoving conformal distance. Assuming a flat  $\Lambda$ CDM universe this can be written as:

$$r(z) = \frac{c}{H_0} \int_0^z \frac{dz'}{\sqrt{\Omega_{m0}(1+z')^3 + \Omega_{\Lambda 0}}}. \tag{B3}$$

and thus  $r_{ls} \equiv r(z_{ls})$  refers to the comoving radius at last scattering from the observer at  $z = 0$ .

As done with the temperature perturbations, we can expand the lensing potential into multipole moments:

$$\phi(\hat{\mathbf{n}}) = \sum_{\ell m} \phi_{\ell m} Y_{\ell}^m(\hat{\mathbf{n}}). \tag{B4}$$

By applying eq. (A3) into eq. (B1) and carrying out the calculations we get an explicit expression for the lensing  $a_{\ell}^m$  coefficients:

$$\begin{aligned}
a_{\ell}^{mL} &= a_{\ell}^{mP} + \sum_{\ell' \ell'' m' m''} (-1)^{m+m'+m''} \mathcal{G}_{\ell \ell' \ell''}^{-m m' m''} \\
&\times \frac{\ell'(\ell'+1) - \ell(\ell+1) + \ell''(\ell''+1)}{2} a_{\ell'}^{m' P*} \phi_{\ell''}^{*-m''}
\end{aligned} \tag{B5}$$

being  $\mathcal{G}_{\ell \ell' \ell''}^{m m' m''}$  the Gaunt integral defined in equation(A10).

- 
- [1] N. Bartolo, E. Komatsu, S. Matarrese, and A. Riotto, Phys. Rep. **402**, 103 (2004), arXiv:astro-ph/0406398.
- [2] L. Verde, L. Wang, A. F. Heavens, and M. Kamionkowski, **313**, 141 (2000), arXiv:astro-ph/9906301.
- [3] X. Luo, The Astrophysical Journal **427**, L71 (1994).
- [4] D. N. Spergel and D. M. Goldberg, Physical Review D **59**, 103001 (1999), arXiv:astro-ph/9811252.
- [5] D. M. Goldberg and D. N. Spergel, Physical Review D **59**, 103002 (1999), arXiv:astro-ph/9811251.
- [6] E. Komatsu, ArXiv Astrophysics e-prints (2002), arXiv:astro-ph/0206039.
- [7] L. Verde and D. N. Spergel, Physical Review D **65**, 043007 (2002), arXiv:astro-ph/0108179.
- [8] A. Cooray and W. Hu, Astrophys. J. **548**, 7 (2001), arXiv:astro-ph/0004151.
- [9] P. Serra and A. Cooray, Phys. Rev. D **77**, 107305 (2008), 0801.3276.
- [10] D. Hanson, K. M. Smith, A. Challinor, and M. Liguori, ArXiv e-prints (2009), 0905.4732.
- [11] E. Komatsu and D. N. Spergel, Phys. Rev. D **63**, 063002 (2001), arXiv:astro-ph/0005036.
- [12] F. Giovi, C. Baccigalupi, and F. Perrotta, Physical Review D **68**, 123002 (2003), arXiv:astro-ph/0308118.
- [13] F. Giovi, C. Baccigalupi, and F. Perrotta, Physical Review D **71**, 103009 (2005), arXiv:astro-ph/0411702.
- [14] A. P. S. Yadav and B. D. Wandelt, Physical Review Letters **100**, 181301 (2008), 0712.1148.
- [15] D. N. Spergel *et al.*, **170**, 377 (2007), arXiv:astro-ph/0603449.
- [16] P. Creminelli, L. Senatore, M. Zaldarriaga, and M. Tegmark, Journal of Cosmology and Astro-Particle Physics **3**, 5 (2007), arXiv:astro-ph/0610600.
- [17] E. Komatsu *et al.*, **180**, 330 (2009), 0803.0547.
- [18] L. Senatore, K. M. Smith, and M. Zaldarriaga, ArXiv e-prints (2009), 0905.3746.
- [19] D. S. Salopek and J. R. Bond, Phys. Rev. D **42**, 3936 (1990).
- [20] A. Gangui, F. Lucchin, S. Matarrese, and S. Mollerach, Astrophys. J. **430**, 447 (1994), arXiv:astro-ph/9312033.
- [21] J. Maldacena, Journal of High Energy Physics **5**, 13 (2003), arXiv:astro-ph/0210603.
- [22] V. Acquaviva, N. Bartolo, S. Matarrese, and A. Riotto, Nuclear Physics B **667**, 119 (2003), arXiv:astro-ph/0209156.
- [23] J. R. Fergusson and E. P. S. Shellard, ArXiv e-prints (2008), 0812.3413.
- [24] M. Liguori, F. K. Hansen, E. Komatsu, S. Matarrese, and A. Riotto, Physical Review D **73**, 043505 (2006).
- [25] P. Creminelli, L. Senatore, and M. Zaldarriaga, JCAP0703 **019** (2007).
- [26] D. H. Lyth, C. Ungarelli, and D. Wands, Physical Review D **67**, 023503 (2003).
- [27] K. Koyama, S. Mizuno, F. Vernizzi, and D. Wands, JCAP **0711**, 024 (2007).
- [28] E. I. Buchbinder, J. Khoury, and B. A. Ovrut, Physical Review D **76**, 123503 (2007).
- [29] N. Arkani-Hamed, P. Creminelli, S. Mukohyama, and

- M. Zaldarriaga, *Journal of Cosmology and Astro-Particle Physics* **4**, 1 (2004), arXiv:hep-th/0312100.
- [30] M. Alishahiha, E. Silverstein, and D. Tong, *Physical Review D* **70**, 123505 (2004).
- [31] R. K. Sachs and A. M. Wolfe, *Astrophysical Journal* **147**, 73 (1967).
- [32] M. J. Rees and D. W. Sciama, *Nature* **217**, 511 (1968).
- [33] R. A. Sunyaev and I. B. Zeldovich, *ARA&A* **18**, 537 (1980).
- [34] E. Komatsu *et al.*, *The Astrophysical Journal* **148**, 119 (2003).
- [35] A. Cooray and W. Hu, *Astrophysical Journal* **534**, 533 (2000), arXiv:astro-ph/9910397.
- [36] R. E. Smith *et al.*, *MNRAS* **341**, 1311 (2003), arXiv:astro-ph/0207664.
- [37] <http://camb.info/>.
- [38] J. A. Peacock and S. J. Dodds, *MNRAS* **280**, L19 (1996), arXiv:astro-ph/9603031.
- [39] C.-P. Ma, R. R. Caldwell, P. Bode, and L. Wang, **521**, L1 (1999), arXiv:astro-ph/9906174.
- [40] U. Seljak and M. Zaldarriaga, (1996).
- [41] A. Gangui and J. Martin, *Physical Review D* **62**, 103004 (2000).
- [42] J. P. Ostriker and E. T. Vishniac, *Astrophysical Journal letters* **306**, L51 (1986).
- [43] A. H. Jaffe and M. Kamionkowski, *Phys. Rev. D* **58**, 043001 (1998), arXiv:astro-ph/9801022.
- [44] A. P. S. Yadav, E. Komatsu, and B. D. Wandelt, *Astrophys. J.* **664**, 680 (2007), arXiv:astro-ph/0701921.
- [45] A. J. S. Hamilton, P. Kumar, E. Lu, and A. Matthews, *Astrophysical Journal Letters* **374**, L1 (1991).
- [46] Y.-C. Cai, S. Cole, A. Jenkins, and C. Frenk, p. 648 (2009), 0809.4488.
- [47] P. Cabella *et al.*, **358**, 684 (2005), arXiv:astro-ph/0406026.
- [48] E. Komatsu, D. N. Spergel, and B. D. Wandelt, *Astrophys. J.* **634**, 14 (2005), arXiv:astro-ph/0305189.
- [49] D. Nitta, E. Komatsu, N. Bartolo, S. Matarrese, and A. Riotto, *Journal of Cosmology and Astro-Particle Physics* **5**, 14 (2009), 0903.0894.
- [50] D. Munshi and A. Heavens, *ArXiv e-prints* (2009), 0904.4478.